ANTENNAS FOR SUB-MILLIMETRE WAVE RECEIVERS

Joakim F. Johansson and **Nicholas D. Whyborn**

Department of Radio & Space Science
with Onsala Space Observatory

Pranay Raj Acharya, **Hans Ekström**, **Stellan W. Jacobsson**, and **Erik L. Kollberg**

Department of Applied Electron Physics

Chalmers University of Technology
S-412 96 Gothenburg
Sweden

ABSTRACT

This paper reports on investigations of two antenna types which are suitable for implementation at sub-millimetre wavelengths; the diagonal horn and the sandwiched tapered slot antenna.

The diagonal horn is studied theoretically by expanding the aperture electric field into Gauss-Hermite modes. A few of these modes are then used to model the radiation pattern. The results indicate that the fraction of the power radiated into the fundamental Gaussian mode is about 84 %. About 10 % of the power is radiated in the cross-polarised component. Radiation patterns for a 4 x 4 diagonal horn array, measured at 100 GHz, show good agreement with the theoretical predictions.

The sandwiched tapered slot antenna consists of a slotline antenna which is sandwiched between thick quartz super- and substrates. An elliptical lens is used to collimate the beam. Model experiments have been performed at 30 and 350 GHz. The radiation patterns are worse at the higher frequency, probably due to alignment problems.

1. INTRODUCTION

Commonly used millimetre wave feed antennas, *e.g.* corrugated horns, become very difficult to realize at sub-millimetre wavelengths. The corrugated horns radiate an almost perfect Gaussian beam [1], but the tolerances needed are at the limit of what can be achieved using normal fabrication methods. Some feed types are easier to make, but, as always, there is no such thing as a free lunch. Pyramidal and conical horns exhibit a lack of symmetry in the cardinal planes of the radiation pattern which makes them unsuitable for launching Gaussian beams. The pyramidal horn has the added inconvenience of astigmatism, *i.e.* the phase centres for the E- and H-planes do not generally coincide (*cf.* [2]). The need for an alternative to these horns at sub-millimetre wavelengths is evident.

We have investigated the so-called diagonal horn (*cf.* [2,3]), and it seems to be an interesting candidate for sub-millimetre feeds. The diagonal horn antenna is shown in the following sections to be quite an efficient Gaussian beam launcher. One marked advantage with this horn type is the ease with which it can be machined. When using waveguide technology at millimetre and sub-millimetre wavelengths it is quite common that the mixer is made in the so-called split-block technique. The component is machined in two halves, and when joined together the extra losses are relatively small. The diagonal horn lends itself to this technique (see Figure 0).

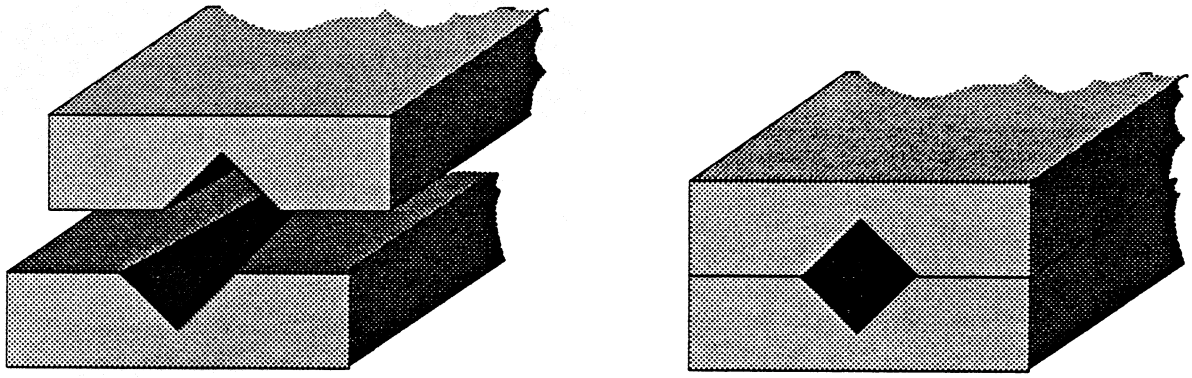

Figure 0. A diagonal horn made in the split-block technique.

The tapered slot antenna is an open structure antenna which radiates a beam in the endfire direction (along the substrate). Classical tapered slot antennas require thin substrates (of the order of $<\approx$ 10 μm at 350 GHz).

One way to solve the substrate problem is to sandwich the antenna between a ***thick*** substrate and superstrate, and then use an elliptical lens to decrease the beamwidth. Results from model experiments at 30 and 350 GHz are presented in the third section of this paper. The results show that it is difficult to achieve good agreement between these two experiments, which is probably due to the stringent tolerance requirements at the sub-millimetre frequency.

2. THE DIAGONAL HORN

The diagonal horn has the following electrical field distribution in the aperture [2, 3] (see Fig. 1 for reference):

$$E_{ap} = E_o\left[\hat{x}\cos\frac{\pi y}{2a} + \hat{y}\cos\frac{\pi x}{2a}\right]e^{jk\delta} \qquad |x|<a \quad |y|<a$$
$$k\delta = \frac{2\pi}{\lambda}\left[\frac{2a^2 - x^2 - y^2}{2L}\right] \tag{1}$$

This means that the field consists of two orthogonal TE_{10} modes, the power evenly distributed between them. This set of modes must be excited somehow. Love [3] used a circular transition from TE_{10}, but the transition seems rather uncritical, and a direct transition from the rectangular waveguide is good enough for most purposes. The aperture equi-phase surface can be assumed to be a sphere centred at the horn apex, and is here approximated by a paraboloid. These assumptions are probably not too wrong, at least not for long horns.

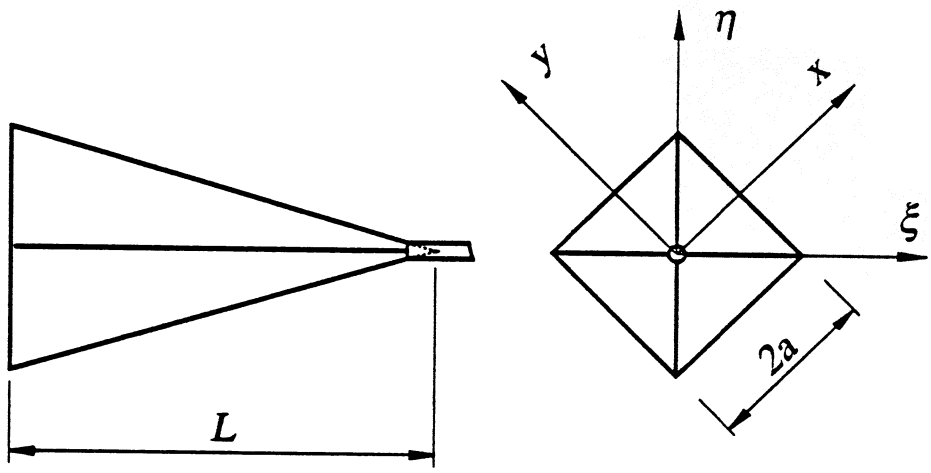

Figure 1. The geometry of the diagonal horn.

The aperture field is seen to have the desired symmetry properties by introducing the following auxiliary coordinate system:

$$\xi = \frac{x-y}{\sqrt{2}} \qquad \eta = \frac{x+y}{\sqrt{2}} \tag{2}$$

Combining Eqns. 1 and 2 yields the following:

$$E_\eta = \hat{\eta}\cdot\boldsymbol{E}_{ap} = \sqrt{2}\,E_o \cos\frac{\pi\xi}{2\sqrt{2}a}\cos\frac{\pi\eta}{2\sqrt{2}a}e^{jk\delta} = \frac{E_o}{\sqrt{2}}\left[\cos\frac{\pi y}{2a} + \cos\frac{\pi x}{2a}\right]e^{jk\delta}$$
$$E_\xi = \hat{\xi}\cdot\boldsymbol{E}_{ap} = \sqrt{2}\,E_o \sin\frac{\pi\xi}{2\sqrt{2}a}\sin\frac{\pi\eta}{2\sqrt{2}a}e^{jk\delta} = \frac{E_o}{\sqrt{2}}\left[\cos\frac{\pi y}{2a} - \cos\frac{\pi x}{2a}\right]e^{jk\delta} \quad (3)$$

The co-polarised aperture field (η-directed) is thus symmetric with respect to the $\xi\eta$ coordinate system. The cross-polarised aperture field component (ξ-directed) is anti-symmetric, and the feed thus has no boresight cross-polarisation (note that we here use the so-called Ludwig's 1st definition [4] for the polarisation). The aperture field components are shown in Fig. 2.

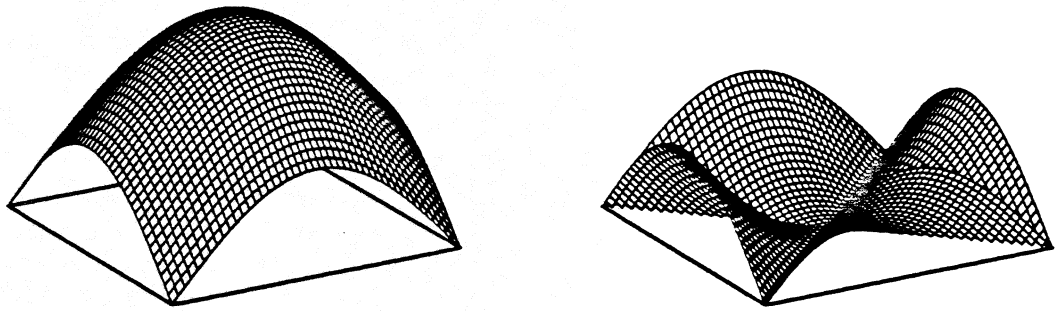

Figure 2. The magnitude of the co- (left) and cross-polarised (right) electric field at the aperture of the horn.

The fraction of the power in the respective components can be found by solving the integrals

$$P_{co} = \int_{-a}^{a}\int_{-a}^{a} |E_\eta|^2\,dxdy \qquad P_{cr} = \int_{-a}^{a}\int_{-a}^{a} |E_\xi|^2\,dxdy \quad (4)$$

where the electric field components are given by Eqn. 3. The numerical results are given by

$$\frac{P_{co}}{P_{co}+P_{cr}} = \frac{1+\frac{8}{\pi^2}}{2} \approx 0{,}9052847$$
$$\frac{P_{cr}}{P_{co}+P_{cr}} = \frac{1-\frac{8}{\pi^2}}{2} \approx 0{,}0947153 \quad (5)$$

It is seen that the cross-polarised part is quite large (≈ 10 %), and this might be excessive for some applications. However, in many cases, this cross-polarised components could be dumped in a termination through the use of a polarising grid. The loss one would encounter by dropping the cross-polarised part is then ≈ 0,43 dB.

2.1. GAUSSIAN MODE EXPANSION

A powerful technique to study the radiation pattern of an aperture antenna is to expand the aperture field into Gauss-Hermite or Gauss-Laguerre functions (*cf.* [1, 5, 6]).

The electric field for a well-collimated beam can be written as

$$E(x,y,z) = \frac{w_A}{w(z)} e^{-jk[z-z_A]} e^{j[\Phi(z)-\Phi_A]} e^{-jk[x^2+y^2]/2R(z)} \cdot \sum_{m=-\infty}^{\infty} \sum_{n=-\infty}^{\infty} \mathcal{K}_{mn} e^{j(m+n)[\Phi(z)-\Phi_A]} \tilde{H}_m\left[\frac{\sqrt{2}x}{w(z)}\right] \tilde{H}_n\left[\frac{\sqrt{2}y}{w(z)}\right] \tag{6}$$

where a modified Hermite function, defined by

$$\tilde{H}_m(x) \triangleq \frac{e^{-x^2/2}}{\sqrt{2^m m!}} H_m(x) \tag{7}$$

is used to get a compact notation.

The beam parameters in Eqn. 6 are given by (*cf.* [6])

$$\begin{aligned} w(z) &= w_o\sqrt{1+[z/z_c]^2} \\ R(z) &= z\left[1+[z_c/z]^2\right] \qquad z_c = \frac{\pi w_o^2}{\lambda} \\ \Phi(z) &= \arctan\frac{z}{z_c} \end{aligned} \tag{8}$$

where w denotes the beam waist radius, R the phase radius of curvature, z_c the confocal distance, and Φ the so-called phase slip. Returning to Eqn. 6, one observes that w and R are common to all modes, whereas the phase slip Φ gets progressively multiplied for higher order modes.

If one now has an aperture field E_A where most of the phase variation can be contained in a spherical phase factor, *viz.*

$$E_A(x,y) = E(x,y,z_A) = g(x,y)\, e^{-j\,k[x^2+y^2]/2R_A} \tag{9}$$

then Eqn. 6 collapses into a very convenient form.

Using the orthogonality properties of Hermite polynomials [7], and some algebraic manipulations, the coefficients $\mathcal{K}_{mn}$ are given by

$$\mathcal{K}_{mn} = \frac{2}{\pi w_A^2} \int_{-\infty}^{\infty}\int g(x,y)\, \tilde{H}_m\left[\frac{\sqrt{2}x}{w_A}\right] \tilde{H}_n\left[\frac{\sqrt{2}y}{w_A}\right] dxdy \tag{10}$$

If now the $g(x,y)$ function is real-valued, one avoids all numerical problems due to rapid phase variations in the integrand.

The diagonal horn has no phase variation over the aperture except for the spherical part. It thus lends itself to this Gauss-Hermite analysis. The $g(x,y)$ functions for the co- and cross-pol parts are given by Eqn. 3.

The mode power content is given by

$$\frac{P_{mn}}{P_{tot}} = \frac{\pi w_A^2}{2} \frac{|\mathcal{K}_{mn}|^2}{\int_{-\infty}^{\infty}\int |g(x,y)|^2\, dxdy} \tag{11}$$

and the results for the diagonal horn are the following expressions

$$\frac{P^{co}_{mn}}{P_{tot}} = \frac{64}{\pi}\frac{a^2}{w_A^2}\left|\int_0^1 \int_0^{1-u} \cos\frac{\pi u}{2}\cos\frac{\pi v}{2}\, \tilde{H}_m\left[\frac{2a}{w_A}u\right] \tilde{H}_n\left[\frac{2a}{w_A}v\right] dudv\right|^2 \quad \textit{Even } m, n \tag{12a}$$

$$\frac{P^{\sigma}_{mn}}{P_{tot}} = \frac{64}{\pi}\frac{a^2}{w_A^2}\left|\int_0^1 \int_0^{1-u} \sin\frac{\pi u}{2}\sin\frac{\pi v}{2}\, \tilde{H}_m\left[\frac{2a}{w_A}u\right] \tilde{H}_n\left[\frac{2a}{w_A}v\right] dudv\right|^2 \quad \textit{Odd } m, n \tag{12b}$$

The expressions in Eqns. 12a and 12b can be simplified for a few simple cases by breaking down the double integrals into single integrals. The result for the fundamental Gaussian is

$$\frac{P^{co}_{00}}{P_{tot}} = \frac{16}{\pi}\frac{a^2}{w_A^2}\left|\int_0^1 \cos\frac{\pi t}{2}\, e^{-\left[at/w_A\right]^2} dt \int_0^1 e^{-\left[at/w_A\right]^2} dt\right|^2 \tag{13}$$

The choice of the ratio w_A/a is in principle arbitrary, but Occam's Razor‡ tells us that the most natural choice is to maximise the fundamental mode coupling [8], *i.e.*

$$\frac{\partial}{\partial \frac{w_A}{a}}\left[\frac{P_{00}^{co}}{P_{tot}}\right] = 0 \tag{14}$$

The coupling has a maximum at $w_A/a \approx 0{,}86$. An optimisation program gave the following results (correct to six decimal places):

$$\begin{cases} \kappa \triangleq \left.\frac{w_A}{a}\right|_{opt} \approx 0{,}863191 \\ \left.\frac{P_{00}^{co}}{P_{tot}}\right|_{opt} \approx 0{,}843025 \end{cases} \tag{15}$$

The diagonal horn thus has quite a high fundamental Gaussian mode content. The mode content for the higher order co-polar and cross-polar components is shown in Table I.

	n = 0	n = 2	n = 4	n = 6	n = 8
m = 0	0,8430	$3{,}655 \cdot 10^{-18}$	0,005405	0,0009189	$5{,}110 \cdot 10^{-6}$
m = 2	☆	0,01620	0,003339	$6{,}859 \cdot 10^{-6}$	0,0003185
m = 4	☆	☆	$1{,}562 \cdot 10^{-5}$	0,001012	0,0009922
m = 6	☆	☆	☆	0,001356	0,0005954
m = 8	☆	☆	☆	☆	$7{,}364 \cdot 10^{-5}$

	n = 1	n = 3	n = 5	n = 7	n = 9
m = 1	0,04848	0,007725	0,0004141	$1{,}117 \cdot 10^{-5}$	$4{,}800 \cdot 10^{-5}$
m = 3	☆	$6{,}037 \cdot 10^{-5}$	0,001545	0,001380	0,0006026
m = 5	☆	☆	0,002060	0,0008870	0,0001456
m = 7	☆	☆	☆	0,0001112	$2{,}909 \cdot 10^{-5}$
m = 9	☆	☆	☆	☆	0,0002786

Table I *The power fraction for the mn^{th} co- (top) and cross-pol modes (bottom). The stars denote redundant information.*

‡ "Entia non sunt multiplicanda præter necessitatem" — A philosophical principle devised by William of Occam (c. 1290 – 1349)

Now when we know the optimum waist radius, it is easy to find the equivalent Gaussian beam parameters. If one assumes the following (see Figure 3 for reference)

$$w_A = w_o\sqrt{1+\left[z_A/z_c\right]^2} = \kappa a$$

$$R_A = z_A\left[1+\left[z_c/z_A\right]^2\right] = L \qquad z_c = \frac{\pi w_o^2}{\lambda} \tag{16}$$

$$\Phi_A = \arctan\frac{z_A}{z_c} = \arctan\frac{\pi\kappa^2 a^2}{\lambda L}$$

then some algebraic manipulations will yield the results

$$w_o = \frac{\kappa a}{\sqrt{1+\left[\frac{\pi\kappa^2 a^2}{\lambda L}\right]^2}} = \frac{\kappa a}{\sqrt{1+\tan^2\Phi_A}}$$

$$z_A = \frac{L}{1+\left[\frac{\lambda L}{\pi\kappa^2 a^2}\right]^2} = \frac{L}{1+\cot^2\Phi_A} \tag{17}$$

The phase slip Φ_A is again seen to be an important parameter in this analysis.

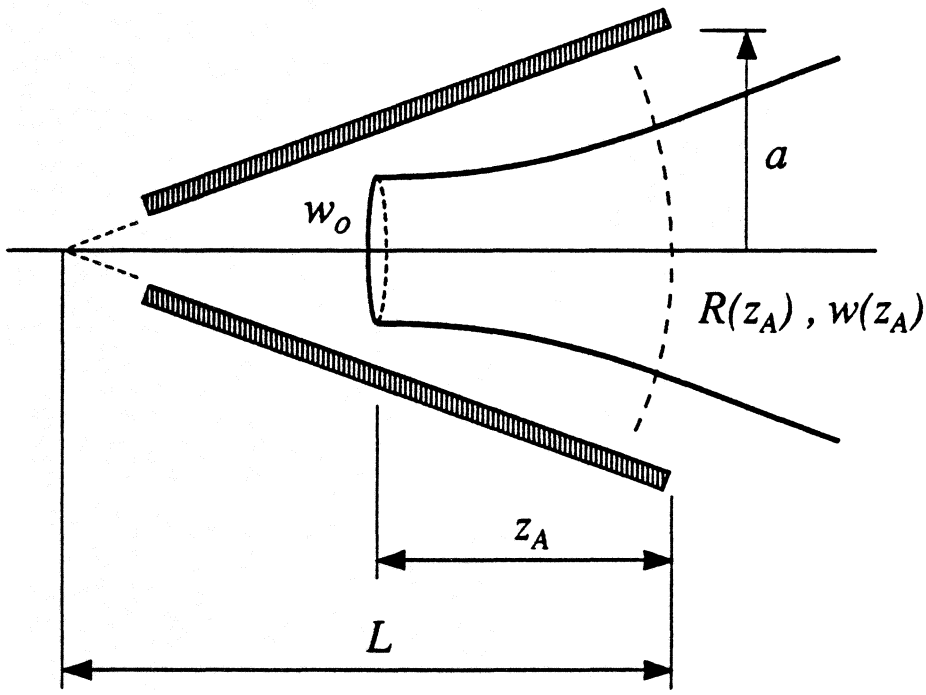

Figure 3. The geometry of the equivalent Gaussian beam

Table I showed that there are just a few terms that contain a significant part of the power, namely the 00, 11, and 22 terms. It is hence possible to devise a simple model for the radiation pattern of the diagonal horn. The far-field radiation pattern is given by (except for an unimportant constant):

$$F_{co}(\theta,\varphi) \approx e^{-2\rho^2}\left|\mathcal{K}_{00} + \frac{1}{2}\mathcal{K}_{22}\, e^{-j4\Phi_A}\left[4\rho^2\cos^2\varphi - 1\right]\left[4\rho^2\sin^2\varphi - 1\right]\right|^2$$

$$F_{cr}(\theta,\varphi) \approx e^{-2\rho^2}\left|\mathcal{K}_{11}\, 4\rho^2\sin\varphi\cos\varphi\right|^2 \qquad (18)$$

$$\rho = \frac{\pi w_o}{\lambda}\tan\theta$$

The coefficients for the optimum waist size (Eqn. 15) are found by numerically evaluating the integral in Eqn. 10, and the coefficients for the model in Eqn. 18 are

$$\frac{\mathcal{K}_{22}}{\mathcal{K}_{00}} \approx -0{,}138628$$

$$\frac{\mathcal{K}_{11}}{\mathcal{K}_{00}} \approx 0{,}239816 \qquad (19)$$

Combining Eqns. 18 and 19 one can draw the conclusion that the far-field radiation pattern is quite rotationally symmetric. The cross-pol level is approximately

$$\frac{e^{-2}\left|2\mathcal{K}_{11}\right|^2}{\left|\mathcal{K}_{00}\right|^2} \approx -15{,}1\ \text{dB} \qquad (20)$$

If the phase slip factor is zero, the radiation pattern will exhibit deep nulls, whereas a non-zero value will yield a more 'smeared' pattern.

It will be shown in the following section that this simplified model is quite accurate.

2.2. MEASUREMENTS

In order to test the theoretical predictions, an array of diagonal horns was manufactured and the radiation patterns were measured. The array is shown in Figure 4. The respective horns are fed by standard waveguide (IEC R-900) and the back side hole patterns match "standard" flanges. A waveguide detector is bolted to the back side. The patterns were measured in an anechoic chamber using a computerised antenna measurement system.

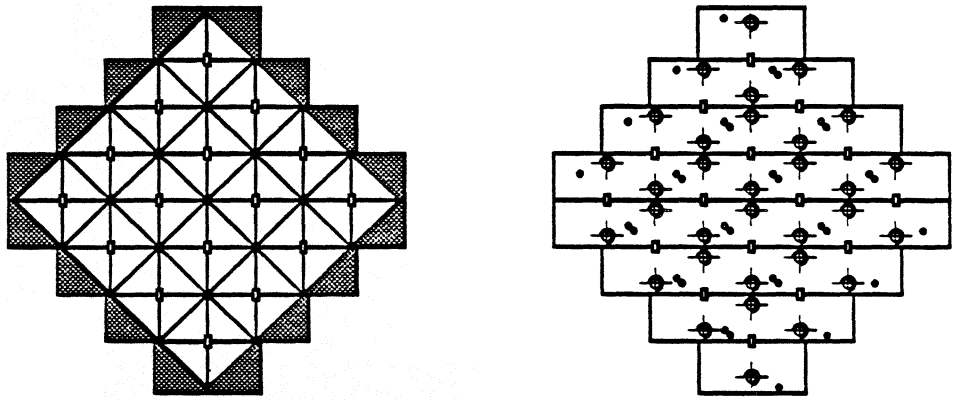

Figure 4 The diagonal horn array.

The horns in the array had the following dimensions:

- $2a = 14{,}0$ mm
- $L = 55{,}0$ mm

The horns were measured at 99 GHz ($\lambda \approx 3{,}03$ mm) and the Gaussian parameters are thus given by (see Eqns. 15, 16, and 17)

- $w_o \approx 4{,}98$ mm
- $z_A \approx 17{,}7$ mm
- $\kappa a \approx 6{,}04$ mm
- $\Phi_A \approx 34{,}54°$

The E-, H-, and D-plane co-pol patterns, as well as the D-plane cross-pol patterns were measured for four of the sixteen horns in the array (see Fig. 5 for reference)

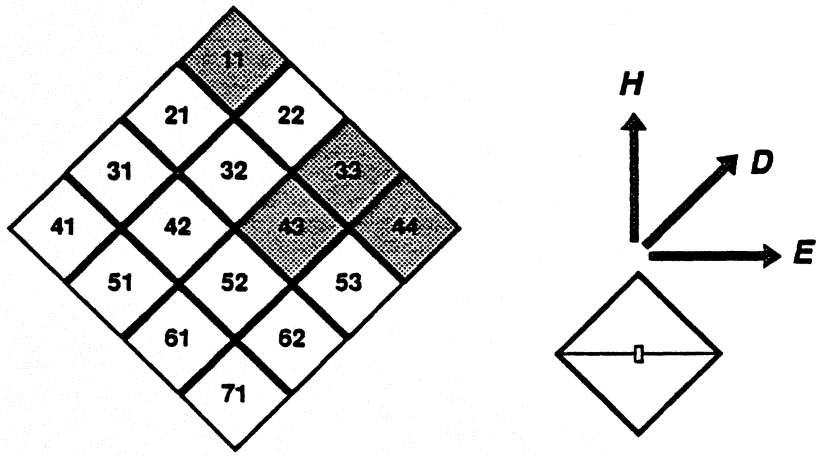

Figure 5. The enumeration of the array elements and the plane definitions. The measured horns are shaded.

Figure 6 shows that the measured radiation pattern is rotationally symmetric down to about -17 dB. The D-plane pattern has a 'shoulder', but except for that the pattern looks nice. The E- and H-plane sidelobes are probably hidden by noise below the -30 dB region. The D-plane cross-pol component is shown in Figure 7. The pattern is a little bit asymmetrical, end shows on-axis cross-polarisation. The reasons for these non-idealities are probably found in the difficulty to accurately set up the antennas at 100 GHz. A small error in feed angle will 'leak' co-pol power into the cross-pol measurement. Any lack of polarisation purity of the transmitting horn might influence the accuracy as well.

The horns do not seem to be especially influenced by being embedded in an array. Figure 8 shows a comparison between four H-plane element patterns. The uniformity is excellent, and one can thus safely use the horns in such an array, without deteriorating the radiation patterns.

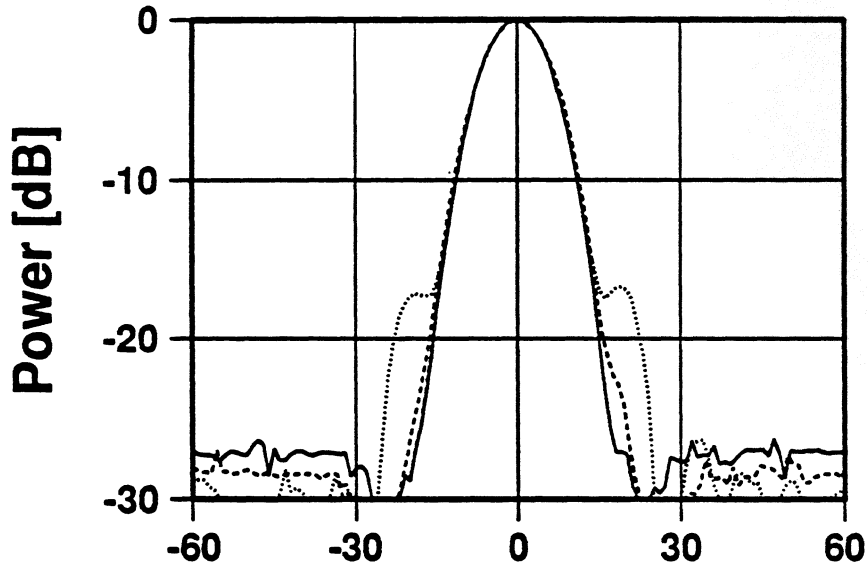

Figure 6. Measured radiation patterns for the H- (solid), E- (dashed), and D-planes (dotted) of a diagonal horn in the array (#33 in Fig. 5).

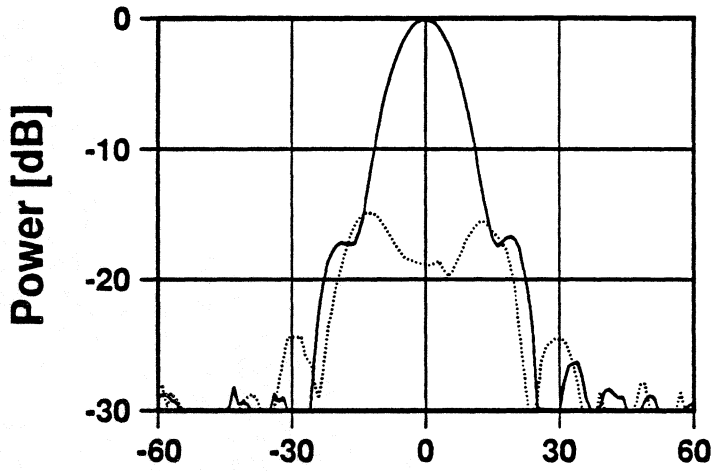

Figure 7. *Measured radiation patterns for the D-plane co-pol (solid) and cross-pol (dotted) components of a diagonal horn in the array (#33 in Fig. 5).*

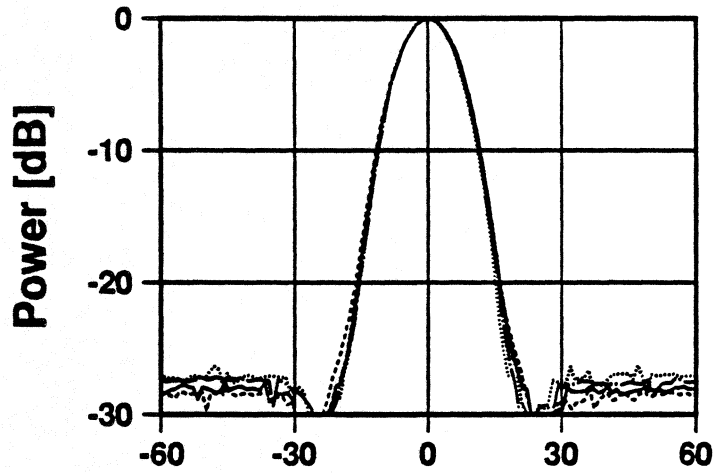

Figure 8. *Comparison between measured H-plane radiation patterns for four different diagonal horn array elements (#11, #33, #43, and #44 in Fig. 5).*

It is quite interesting to compare the measured patterns with the ones predicted by the theoretical model, introduced in Eqn. 18. Figures 9 through 11 show this comparison. The H-plane pattern shows excellent agreement, whereas the theoretical model fails to show the characteristic shoulders in the D-plane (Fig. 10). The cross-pol level (Fig. 11) is predicted to within 1 dB, and the pattern form is qualitatively correct. The simplistic model can hence yield quite a good agreement with measurements.

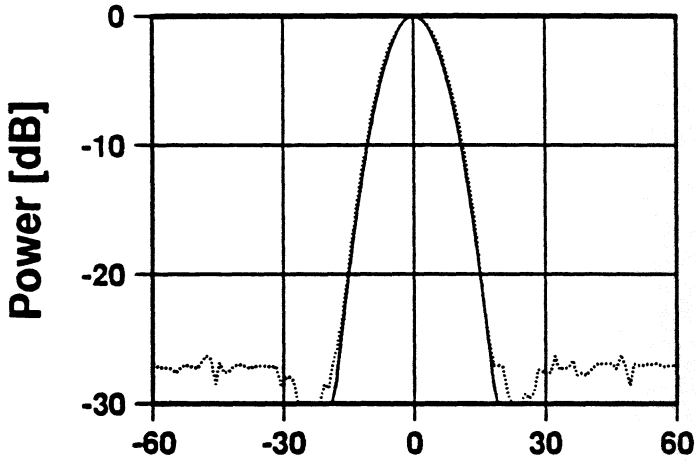

Figure 9. Comparison between measured (dotted) and theoretical (solid) H-plane radiation patterns.

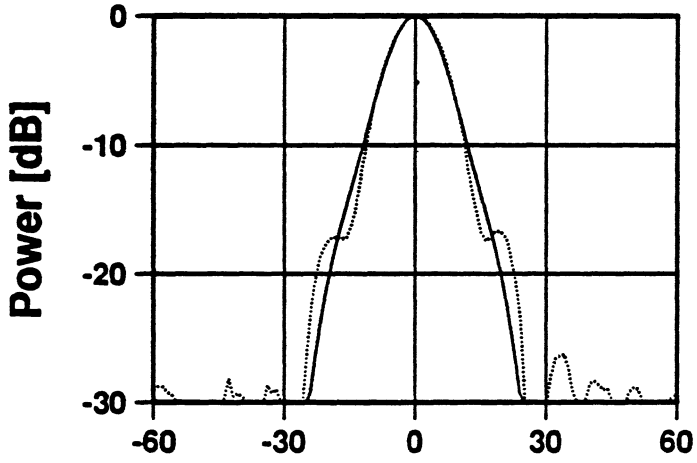

Figure 10. Comparison between measured (dotted) and theoretical (solid) co-pol D-plane radiation patterns.

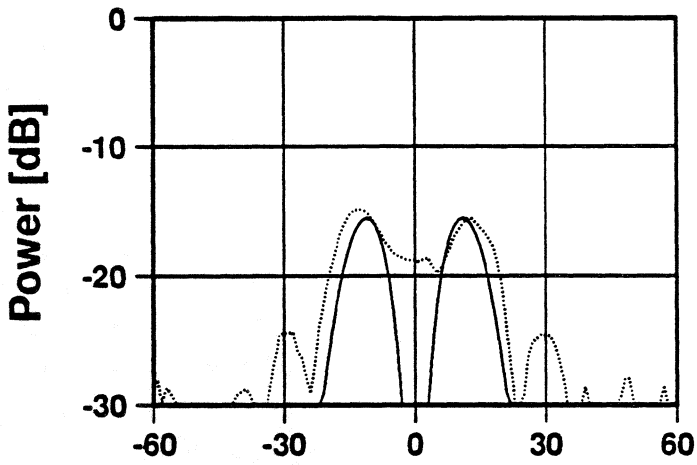

Figure 11. Comparison between measured (dotted) and theoretical (solid) cross-pol D-plane radiation patterns.

3. SANDWICHED TAPERED SLOT ANTENNAS

Various forms of slotline components are attractive, topologically and electrically, for integration with *e.g.* sub-millimetre wave SIS mixers. The thickness of the slotline substrate should be small, so that no surface waves are excited. For a slotline antenna the requirement is even more stringent, and the thickness should, as a rule of thumb, be less than ~ $0.03\,\lambda/(\sqrt{\varepsilon_r}-1)$ (*cf.* [9]). Hence, the required thickness of a quartz substrate at 350 GHz is of the order of < 20 μm. Such thin substrates are difficult to handle as well as to fabricate. In order to avoid these problems, we developed a sandwiched slotline antenna, *i.e.* a slotline antenna sandwiched between two thick dielectric sub-/superstrates. The surrounding of the antenna will then have the same dielectric constant, which is equivalent to a free antenna without any supporting substrate, see Figure 12. It should be noted that sandwich type antennas have also been developed elsewhere (see *e.g.* [10, 11]).

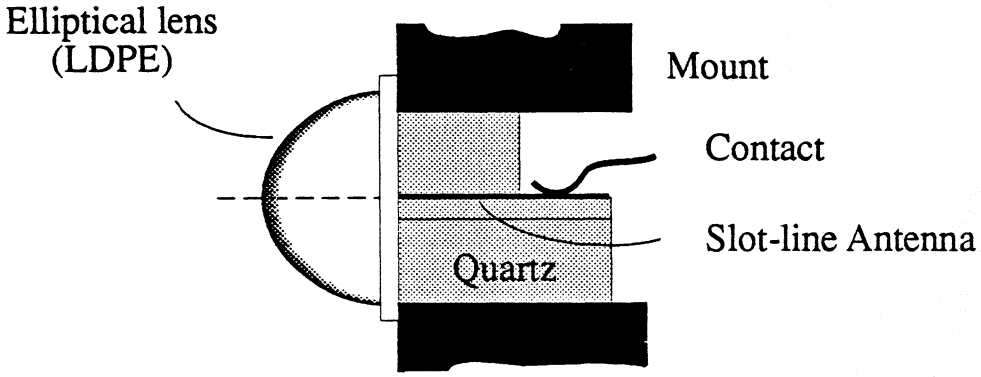

Figure 12. "Artist's view" of the sandwiched slotline antenna, including a beamshaping lens. (side view)

Several 30 GHz scale models were built to evaluate the sandwich concept, see Figure 13. The best antenna found was a slotline antenna of the BLTSA (Broken Linearly Tapered Slotline Antenna) type [12], with an elliptical lens made of low density polyethylene ($\varepsilon_r \approx 2{,}3$), mounted in front of the sandwich. The sidelobe level is typically below -20 dB, and the cross-polarisation in the D-plane is less than -10 dB. Representative E-, H-, and D-plane patterns of this scale model antenna are shown in Figure 14. This scale model antenna was chosen to empirically find suitable dimensions for the sandwiched BLTSA antennas for integration with SIS mixers at 350 GHz.

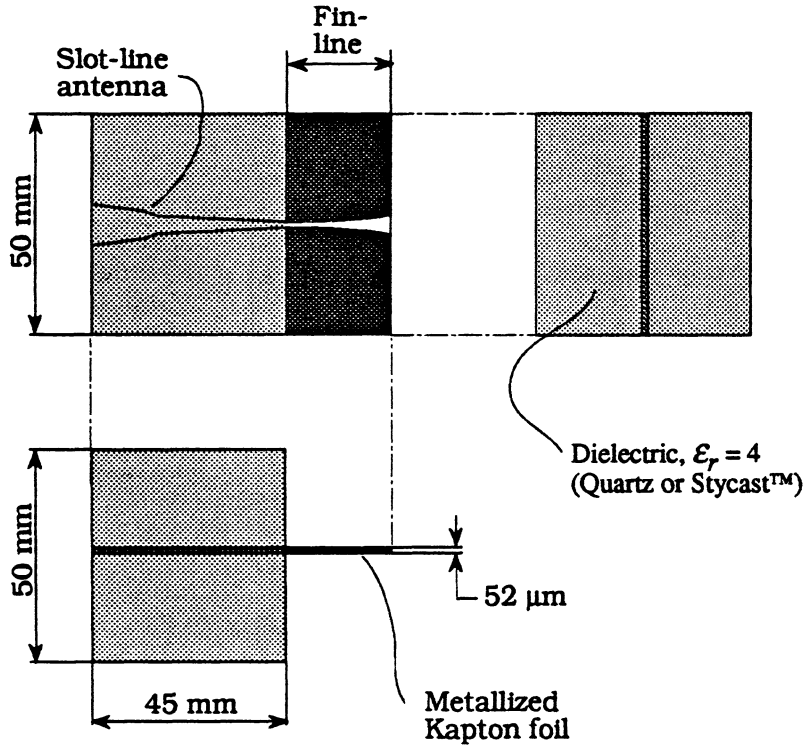

Figure 13. Dimensions of the 30 GHz scale model. Lens not shown.

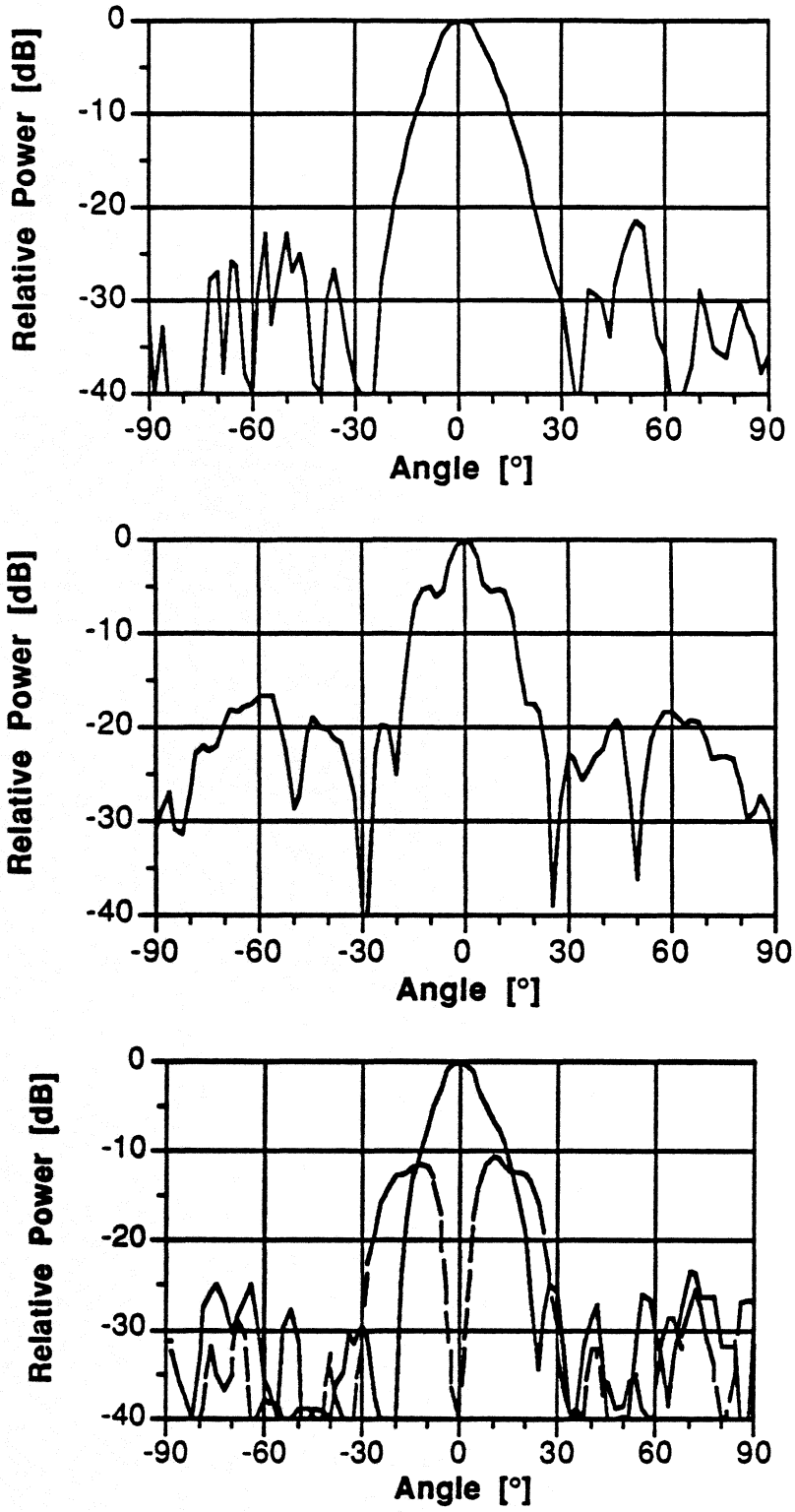

Figure 14. *Antenna diagrams measured at 30 GHz (scale model). The panels show the radiation patterns in the E- (top), H- (middle), and D-plane (bottom), respectively. The D-plane plot shows both co- (solid line) and cross-pol (dashed line) data.*

In order to test the antenna properties at 350 GHz, a slotline antenna and a bismuth bolometer detector (see Figure 15) were integrated on a 0,5 mm thick crystalline quartz substrate and sandwiched between two ~2 mm thick pieces of crystalline quartz.

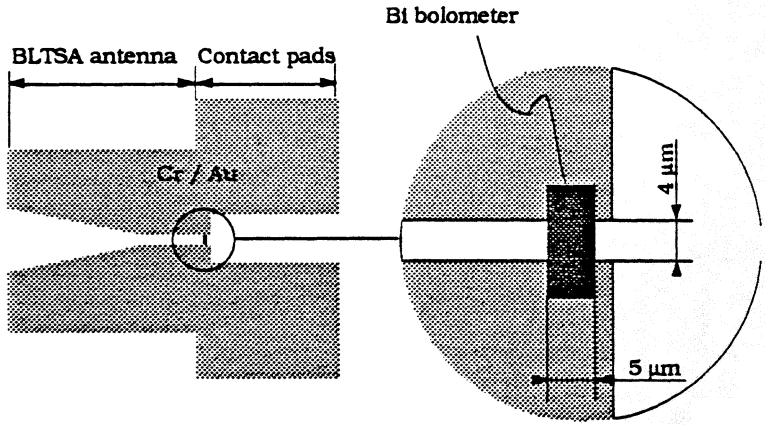

Figure 15. Schematic of a slotline antenna for 350 GHz with an integrated bismuth bolometer. The resistance of the bolometer should match the impedance of the slotline, ~ 50 Ω.

The fabrication of the antenna and the bolometer is straightforward; The antenna (Cr/Au) and the bismuth bolometer are both manufactured by lift-off. The lift-off process gives a smooth gold edge, which is essential for good electrical contact between the bolometer and the antenna. To obtain a uniform bismuth layer the substrate is cooled to approximately –60 °C during the evaporation. The resistance of the bolometer is continuously monitored during evaporation. The evaporation of bismuth is stopped when the bolometer has reached the desired resistance to match the impedance of the antenna.

The measured E- and H- plane antenna patterns for the sandwich slotline antenna at 350 GHz are shown in Figure 16.

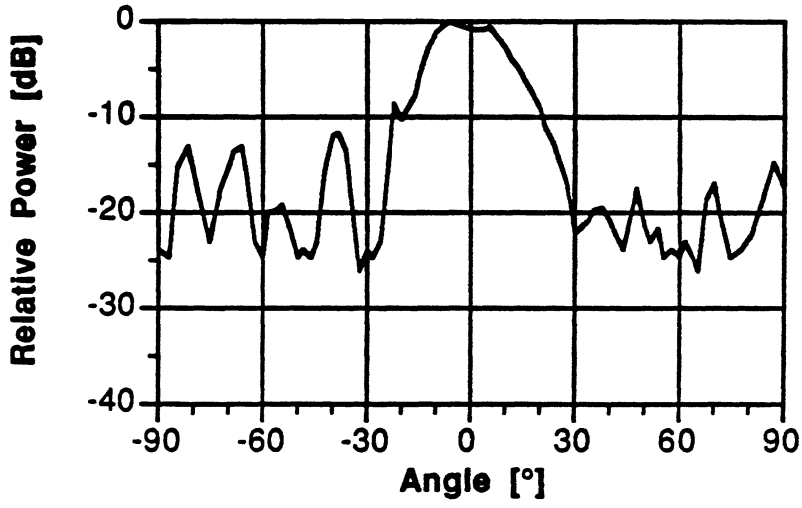

Figure 16a. Measured E- plane antenna pattern for a sandwiched BLTSA antenna at 350 GHz

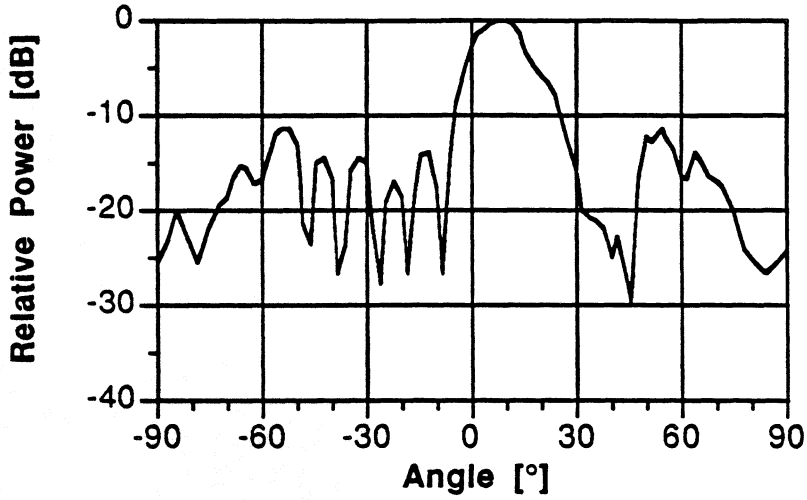

Figure 16b. Measured H- plane antenna pattern for a sandwiched BLTSA antenna at 350 GHz.

At 350 GHz, the sidelobe level in the E-plane is almost 10 dB higher compared to the 30 GHz scale model measurements. In the H-plane the pattern shows more asymmetries, in addition to a 5 dB increase in sidelobe level.

The deteriorated quality of the antenna patterns recorded at 350 GHz, particularly in the H-plane, is most probably due to alignment problems. For instance, the lens has to be accurately aligned (within 50 μm), and it is essential to avoid any air gaps between the quartz pieces.

4. CONCLUSIONS

The diagonal horn antenna has been theoretically investigated. The model using the Gauss-Hermite expansion yields an agreement with measured data which ranges from good to excellent. The horn has a high fundamental Gaussian mode content (≈ 84 %). The design lends itself to conventional millimetre and sub-millimetre construction methods, such as the split-block technique. The small interactions that were seen in the array measurements indicate that the diagonal horn antenna is a strong candidate for focal plane imaging arrays.

The sandwiched tapered slot antenna is a planar feed which can be easily integrated with *e.g.* SIS mixers. The model experiments made at 30 GHz show discrepancies with 350 GHz measurements. The stringent tolerance requirements at sub-millimetre frequencies could at least partly explain these discrepancies.

REFERENCES

[1] R. Wylde, "Optics and Corrugated Feedhorns", IEE Proc.,Vol. 131, Pt. H, No. 4, pp. 258-262, Aug. 1984.

[2] E.I. Muehldorf, "The Phase Center of Horn Antennas", IEEE Trans. Antennas Propagat., Vol. AP-18, No. 6, pp. 753-760, Nov. 1970.

[3] A.W. Love, "The Diagonal Horn Antenna", Microwave J., Vol. V, pp. 117-122, Mar. 1962.

[4] A.C. Ludwig, "The Definition of Cross Polarization", IEEE Trans. Antennas Propagat., Vol. AP-21, No. 1, pp. 116-119, Jan. 1973.

[5] J.A. Murphy and R. Padman, "Phase Centers of Horn Antennas Using Gaussian Beam Mode Analysis", IEEE Trans. Antennas Propagat., Vol. AP-38, No. 8, pp. 1306-1310, Aug. 1990.

[6] P.F. Goldsmith, "Quasi-Optical Techniques at Millimeter and Submillimeter Wavelengths", Ch. 5 in ***Infrared and Millimeter Waves***, Vol. 6, K. Button, Ed., pp. 277-343, Academic Press, 1982.

[7] M. Abramowitz and I.A. Stegun, ***Handbook of Mathematical Functions***, 9th printing, ISBN 0-486-61272-4, Dover Publications, New York.

[8] D.H. Martin, *et al.*, ***Millimetre-Wave Optics*** (Compendium), Queen Mary College, London, UK, 1988.

[9] K.S. Yngvesson, D.H. Schaubert, T.L. Korzeniowski, E.L. Kollberg, T. Thungren, and J.F. Johansson, IEEE Trans. Antennas Propagat., Vol. AP-33, No. 12, pp. 1392-1400, Dec. 1985.

[10] T. L. Hwang, D. B. Rutledge, and S. E. Schwarz, "Planar Sandwiched Antennas for Submillimeter Applications", Appl. Phys. Lett. 34(1), 1 January 1979.

[11] A. Eckart, A.I. Harris and R. Wohlleben, "Scaled Model Measurements of the Sandwiched V-Antenna", Int. J. IR and MM Waves 9, 6 (1988).

[12] P.R. Acharya, J.F. Johansson, and E.L. Kollberg, "Slotline Antennas for Millimeter and Submillimeter Waves", Proc. 20th European Microwave Conf., Budapest, Hungary, Sept. 10-13, 1990, Vol. 1, pp. 353-358.